Thermal expansion measurements in fresh and saline ice using fiber optic strain gauges and multi-point temperature sensors based on Bragg gratings

Aleksey Marchenko[1], Ben Lishman[2], David Wrangborg[1], Torsten Thiel[3]
[1]The University Centre in Svalbard, Longyearbyen, Norway
[2] Institute for Risk and Disaster Reduction,
University College London, London, UK
[3]Advanced Optics Solutions (AOS) GmbH, Dresden, Germany

Thermal expansion measurements in fresh and saline ice using fiber optic strain gauges and multi-point temperature sensors based on Bragg gratings

Aleksey Marchenko[1], Ben Lishman[2], David Wrangborg[1], Torsten Thiel[3]
[1]The University Centre in Svalbard, Longyearbyen, Norway
[2] Institute for Risk and Disaster Reduction,
University College London, London, UK
[3]Advanced Optics Solutions (AOS) GmbH, Dresden, Germany

Abstract
This paper describes the use of Fiber Bragg Grating (FBG) sensors to investigate the thermo-mechanical properties of saline ice. FBG sensors allowed laboratory measurements of thermal expansion of ice samples with a range of different sizes and geometries. The high sampling frequency, accuracy and resolution of the FBG sensors provide good quality data across a temperature range from 0°C to -20°C. Negative values of the effective coefficient of thermal expansion were observed in ice samples with salinity 6ppt, 8ppt and 9.4ppt. A model is formulated under which structural transformations in the ice, caused by temperature changes, can lead to brine transfer from closed pockets to permeable channels, and vice versa. This model is compared to experimental data. Further, in experiments with confined floating ice, heating and thermal expansion due to vertical migration of liquid brine, caused by under-ice water pressure, was observed.

Introduction
Saline ice is a composite material – a solid ice matrix containing liquid and gas inclusions – with a structure which changes under the influence of thermal and mechanical loads. Saline ice consists of pure ice grains, grouped in columns or platelets, and brine pockets and channels. It has been thought that sea ice is impermeable to brine transport when the liquid brine content is less than 5% and is permeable when the brine content is greater than 5% (Weeks and Ackley, 1986). In fact, sea ice always contains porous channels, and liquid brine can migrate through these under the influence of pressure gradients (Golden et al., 2007). Thermal changes influence the permeability of sea ice significantly, as brine freezes into ice on cooling, and ice melts into water on heating. Thus the final state of a saline ice sample subjected to thermal changes is determined not only by initial and final conditions but also by the history of temporal variations and salt fluxes at the boundaries. This means that the thermo-mechanical properties of saline ice samples depend on their size and geometry.

Fresh ice and brine both exhibit typical thermal behavior: they expand when heated and contract when cooled. Saline ice, however, can behave atypically because of phase changes. When brine freezes, this leads to a mean density reduction (since ice is less dense than water), and so cooling can lead to expansion. Similarly, and by the inverse process, heating can lead to contraction. This unusual behavior of saline ice was studied in laboratory experiments and

described by Pettersson (1883) and Malmgren (1927). Their experiments were conducted by immersing a sea ice sample in fluid and measuring the changes in fluid volume as the sample temperature changed. Fluid volume changes were then used to calculate thermal volume expansion coefficients. Johnson and Metzner (1990) note that this procedure assumes no additional fluid is added to the volume of the immersion fluid. This assumption has been found to be invalid, since brine can leak out of the sample and be expelled into the immersion fluid.

Theoretical models for the calculation of the coefficient of thermal expansion of saline ice have been developed by Malmgren (1927) and Cox (1983). Malmgren and Cox made opposing assumptions when formulating the basic equations. Malmgren assumed that brine is never expelled from the sample, and that all salts are trapped in brine pockets inside the sample. Temperature changes therefore cause internal ice melt or brine refreezing. Cox, contrastingly, assumed that the behavior of saline ice is analogous to a pure ice cup filled with liquid brine: both are free to expand and contract independently, and hence phase changes have no effect on the thermal expansion of the ice.

Johnson and Metzner (1990) used a Michelson Interferometer type Laser Dilatometer to measure linear thermal expansion of cylindrical ice samples taken from a sheet of first year congelation sea ice in Harrison Bay, Alaska. Their apparatus included the interferometer along with a sample holder, temperature control unit and computer-controlled data acquisition unit. The diameter of their samples was 38mm and the length was 71.25mm for 2ppt ice, and 69.33mm for 4ppt ice. Optically flat target mirrors were frozen to the front surface of the samples, trimmed parallel with a microtome, and used to control the sample length with the interferometer. They were able to achieve a displacement resolution of 316.4nm, corresponding to a strain resolution of the order of 5×10^{-6}.

Mean and instantaneous values of the thermal expansion coefficient were found to be similar to the fresh ice thermal expansion coefficient of 5×10^{-5} / °C. Their 4ppt ice showed hysteresis when cooled and rewarmed after the initial warming test. Similar effects were observed in the experiments of Butkovich (1959) with fresh water ice, where the coefficient of linear thermal expansion decreased with succeeding runs. Their conclusion was that their results agreed with the analysis of Cox (1983).

Systematic investigations of the thermo-mechanical behavior of saline ice samples were performed, using fiber optic strain and temperature sensors based on Fiber Bragg Gratings, in the cold laboratories of the University Centre in Svalbard, Norway, and University College London, UK, from 2012-2015 (Marchenko et al, 2012, 2013, 2015; Lishman and Marchenko, 2014; Wrangborg et al., 2015). The FBG system used was designed by Advance Optic Solutions GmbH (Germany). The flexibility of the FBG system allowed experiments to be conducted with many different sizes and geometries of ice sample, and with floating ice.

The present paper describes the instrumentation and experimental setups and summarizes experimental results on the measurement of thermal expansion of saline ice. We formulate a new model of the thermal expansion of saline ice, assuming the possibility of structural changes in the ice associated with gradual transformation of closed brine pockets into permeable brine channels, under the influence of temperature changes. Mass changes in the ice with closed brine pockets are estimated using the experimental data. Thermal expansion of saline ice caused by the migration of liquid brine through the ice is also discussed in the paper.

Instrumentation

The fiber type used for this kind of optical sensing are typically standard telecom single-mode fibers (SMF) that are widely used in communications, with an overall diameter of 0.25 mm, and a core diameter of only about 0.01 mm. A Fiber Bragg grating is a periodical index change in the refractive index n along this optical silica fiber's core, formed by an interference pattern of two UV laser beams that the fiber is exposed to. There are various techniques (Othonos 1999) to generate the two coherent beams (Fig. 1a). The index change results from a certain photo-sensitivity of the fiber's core which is due to the presence of some chemical dopants inside the silica's structure, typically Germanium oxide. The interference pattern being generated by two coherent laser beams consists of a periodic UV power modulation along the fiber determined by the incident angle of the two beams. This UV pattern migrates to the fiber core's index change pattern, by the said photo sensitive mechanism.

With a period of less than 10^{-6}mm, areas of higher n alternate with areas of lower n while Δn is relatively small ($\Delta n < 0.001$ *at* $n = 1.45$). Due to the index change, each "grating line" reflects a very small portion of the light wave propagating along the fiber, back to the light source. Although a single reflected portion is negligible compared to the transmitted power, the effect becomes noticeable because the amount of "grating lines" in a conventional FBG is about 4000/mm, and a typical FBG with 10 mm length consists of 40 thousands reflections. If the light's wavelength matches the condition

$$\lambda_{Bragg} = 2 \cdot n_{eff} \cdot \Lambda, \qquad (1)$$

where n_{eff} is the fiber's effective index, λ_{Bragg} is the light's wavelength, and Λ is the index change's period, then all reflected light wave portions are propagating "in-phase" and interfere constructively. Depending on the actual Δn, this results in a typical narrow-band power peak in the reflection spectrum at λ_{Bragg}, and vice versa in a loss in transmission (Fig. 1b). According to equation (1), the reflected wavelength changes with either modifying n_{eff} or Λ .

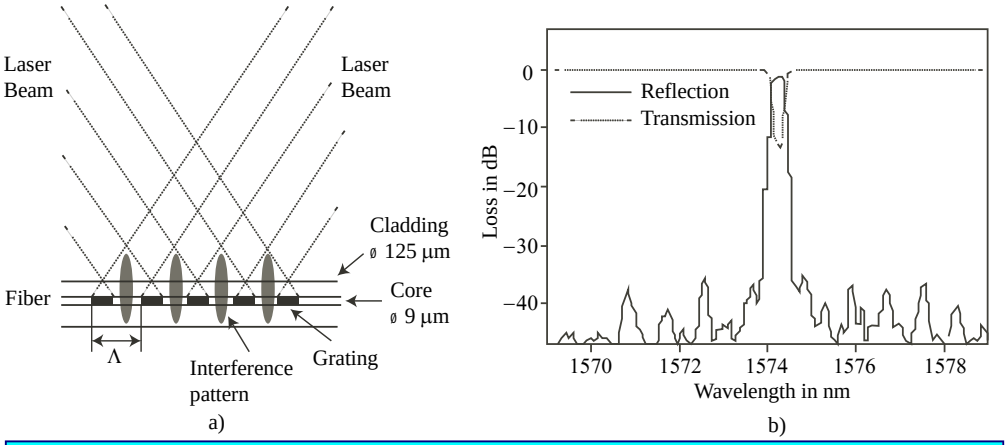

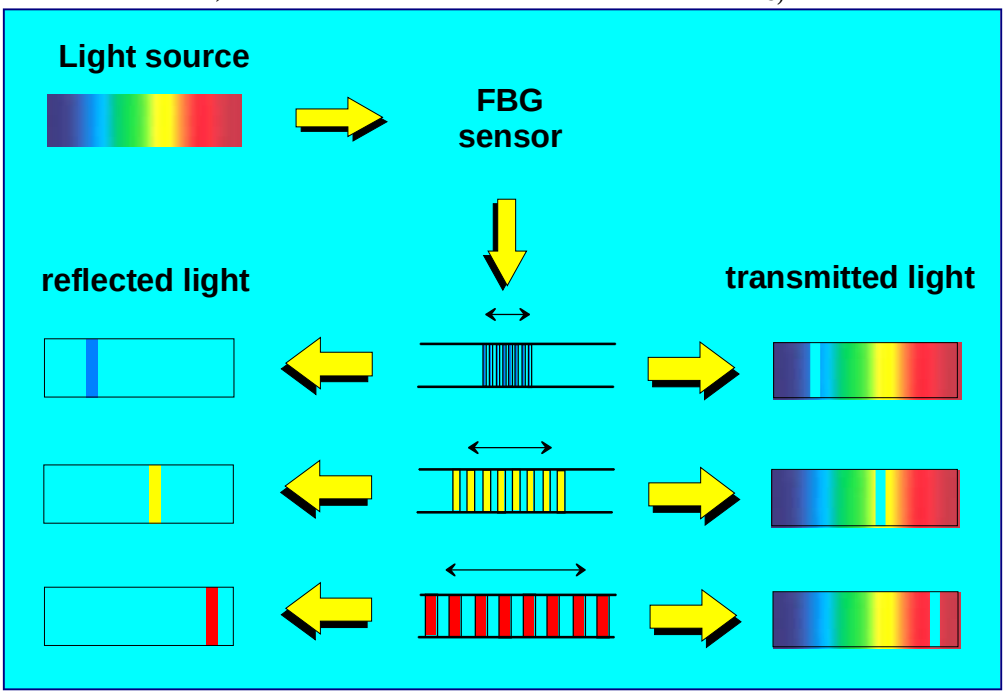

c)

Figure 1. Interference pattern of laser beams in the fiber core during FBG generation (a). Reflected and transmitted signals after the passing of broad band light travelling along the fiber with an FBG inside (b) and a simplified illustration of the strain detection mechanism with a broad band light source containing a continuous spectrum of wavelengths (i.e. colours).

It is easy to see that λ_{Bragg} will change when the fiber is strained or compressed (Fig 1(c)), whereas the effective refractive index is a material property and thus n_{eff} is sensitive to changes in temperature. This sensitivity of the peak wavelength with respect to thermal and mechanical loads allows the usage of FBG as strain and temperature sensors (Rao, 1997; Othonos, 1999). This is now a common field of optical sensing. Several features make the FBG system highly appropriate for geophysical measurements (Ferraro 2002; Mueller, 2006). These features include:

- long term zero-point stability due to the inscribed physical structure;
- transmission of the sensor's signal over distances up to tens of miles;
- a form factor which allows FBG to be embedded into structures;

- good immunity against electromagnetic radiation, and
- ability to cascade and multiplex large numbers of sensors in a network, with a lower complexity than with electrical equivalents.

In our experiment, FBG sensors are practical for measuring the thermal expansion of large samples because, in contrast to standard dilatometers, the fiber can be embedded directly inside the ice sample. An FBG thermistor string and strain sensor are shown in Fig 2. Typical strain resolution for FBG systems is 10^{-6} (1 μstrain) or better, and the accuracy is typically $5 \cdot 10^{-6}$ (5 μstrain). These characteristics are comparable to Michelson Interferometer Laser Dilatometers as used by Johnson and Metzner (1990) and discussed above.

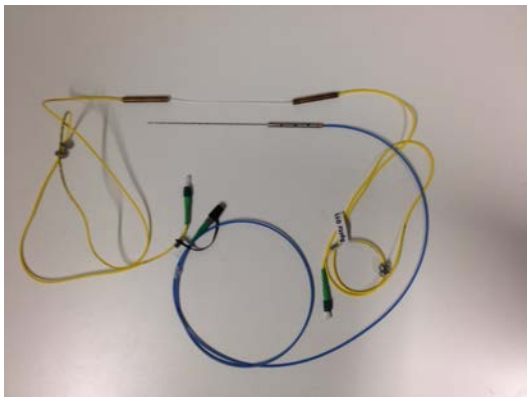

Figure 2. An FBG thermistor string and strain sensor.

The variation ($\Delta\lambda_{Bragg}$) of the peak wavelength caused by the extension ($\Delta L/L$) and the change of the temperature (ΔT) of the sensor is described by the equation

$$\frac{\Delta\lambda}{\lambda} = GF \cdot \frac{\Delta L}{L} + TK \cdot \Delta T \,, \tag{2}$$

where the gauge factor GF=0.719 and a linear temperature coefficient TK=5.5·10^{-6} are the constants obtained from a calibration cycle for our FBG sensors in standard SMF fiber, within a temperature range from -20^{o} C to 0^{o} C.

The variation of the peak wavelength $\Delta\lambda$ is measured with a spectrometer that receives the reflected signal from the FBG sensor. For the calculation of the strain (($\Delta L/L$) according to formula (2) it is necessary to measure the temperature change (ΔT) at the strain sensor's position in order to compensate TK. The temperature measurements can easily be performed with another FBG sensor protected from mechanical deformation, or alternatively with a thermometer. In our experiments, we used FBG strain sensors with a reference peak wavelength in the vicinity of around 1534 nm, and FBG temperature sensors with a reference peak wavelength in the vicinity of around 1565 nm. The strain and temperature sensors were cascaded in one optical fiber. The FBG measurement system's nominal resolution and accuracy in our experiment was 0.08^{o} C and 0.4^{o} C, respectively.

Experiments

Thermal expansion of unconfined ice

Experiments were performed in the cold laboratory of the University Centre in Svalbard (UNIS). Ice was formed in the UNIS ice tank from a mixture of sea water, pumped from a nearby fjord, and fresh water. The salinity of the ice samples varied from 0 to 10 ppt, and the ice had columnar structure. The ice samples had a rectangular shape, with the long dimension around 20cm and the shorter dimensions 5-10cm. The optical fibers with FBG strain sensors had an integrative working length of 20cm that was defined by two brass anchor bolts with nuts and washers. The optical fibers were placed into 2mm-wide cuts that were sawn in the ice samples, and were fastened at the edges of the ice samples with nuts and washers (Fig.3a). The ice block's thermal expansion or shrinkage is therefore transferred to the optical fiber with the FBG inside (this fiber is prestrained to around 0.3% by adjusting the nuts accordingly). The FBG fiber was not frozen into place, since this would allow localized shear around the FBG itself to distort the measurements. The FBG temperature sensor (thermistor string) was encapsulated in a 1mm stainless steel capillary tube and inserted into a drilled hole in the ice sample, next to the FBG strain sensor.

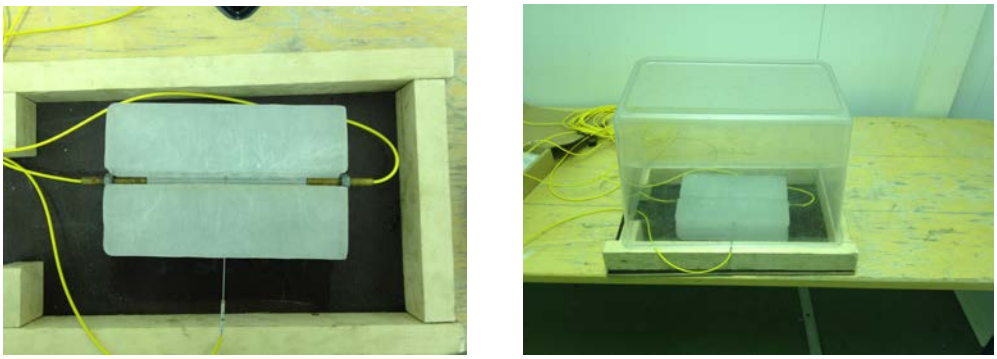

Figure 3. Installation of FBG strain sensor and thermistor string in ice sample (a). Ice sample inside plastic housing (b).

The equipment used in our measurement setup includes a broadband SLED light source with a central wavelength of 1550nm and a bandwidth (FWHM) or ~90nm (AOS GmbH, Germany), a NIR spectrometer 'I-MON 512E-USB 2.0 interrogation monitor' with a detectable spectral width of 1510-1595nm (Ibsen Photonics S/A, Denmark), a PC, and two FBG sensors, one for strain measurement and one for temperature measurement (both AOS GmbH, Germany). The Ibsen monitor is distributed with operating software, including a LabView source code. The experimental schematic is shown in Fig. 4. All electronic devices – the LED source, the spectrometer, and the PC – were installed outside the cold laboratory. Regular optical single-mode cables were used to connect the equipment to the FBG sensors embedded into the ice sample in the cold laboratory.

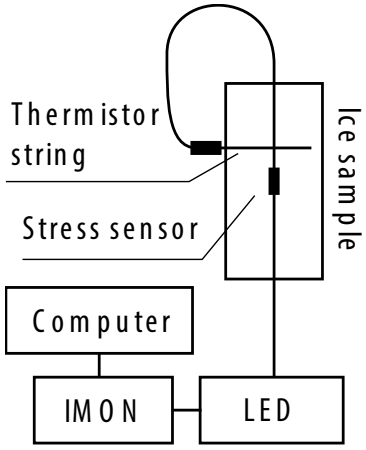

Figure 4. Schematic of experiment for measuring of thermal expansion.

The ice sample was covered by a plastic housing to avoid evaporation (Fig. 3b). The temperature in the cold laboratory (2.5x2.5x1.8m) was changed in increments of 2°C from -20° C to a nominal 0° C, programmed and displayed on the laboratory's control system. Temperature control is provided by a Frigobase Carel system with temperature precision better than 1°C and set point resolution of 0.1°C. Time intervals for the temperature increments were set to 3 hours or greater. Temperature and extension are measured at 1 sample/s. During the experiment, we realized that the actual air temperature close to the ice samples was lower than the displayed temperature by several degrees. We therefore switched off the cooling system to allow the room to warm, resulting in an environmental temperature of -3°C.

Ice salinity was measured with a Mettler Toledo Seven Pro conductivity meter SG7, with resolution 0.01ppt. The salinity of the ice samples was measured before and after the experiments. In some experiments, multiple 'dummy' samples are kept under the same conditions as the strain-gauged sample: these samples can then be used to measure changes in salinity during the experiments.

Thermal expansion of confined ice

A series of experiments were undertaken in the cold rooms of University College London. The FBG strain sensor was used to measure the linear strain in ice samples of cylindrical shape under various conditions. The ice was formed between two steel pipes: an outer pipe with inside diameter 11cm, and an inner pipe with outside diameter 2cm. Fresh ice was made from London tap water; saline ice from the same, with 8ppt NaCl added. The samples were formed in layers, so that up to 1cm depth of water was added and allowed to freeze before the next layer was formed. No evidence was seen of supercooled water or large bubbles within these layers. The experiments are conducted in air.

Ice samples were tested in three conditions: unconstrained, constrained within one pipe, and constrained between two pipes (in the first two cases, pipes were removed after forming by briefly warming). These conditions are illustrated in Fig. 5. The pipe has length 180mm, and the samples are milled 5mm from either end of the pipe, such that the initial ice sample has two flat parallel ends 190mm

apart. On these flat ends we place an aluminium spacer of width 4mm which supports the FBG strain sensor, so that expansion in the ice in the along-pipe (z) direction stretches the sensor.

Temperatures are measured using the FBG 12-thermistor string inserted through a drilled hole in the ice (or ice and pipe), such that temperatures are recorded through the sample in the x-direction. The temperature used for calibration of the strain sensor is that closest to the sensor: in this case, thermistor 7. For calculation of thermal expansion, we use the average of thermistors 1-5, which gives a mean value through the ice, but eliminates the thermistors in the air, which respond much faster to temperature changes in the room. Temperature and extension are measured at 1 sample/s. The entire apparatus is shown in a photograph in Fig. 6.

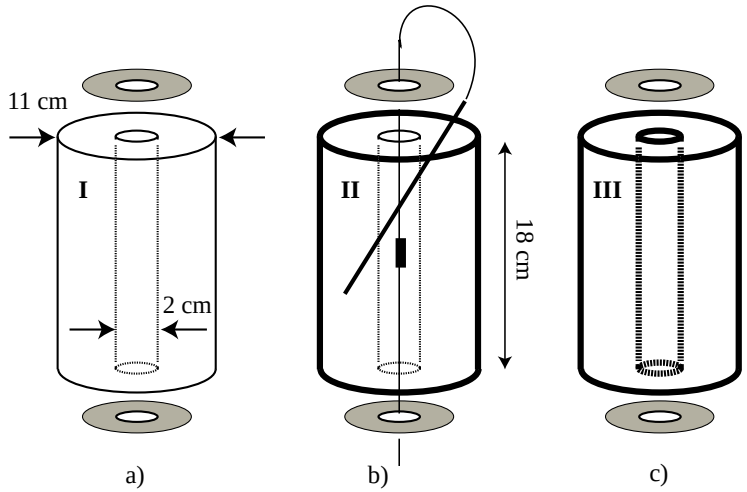

Figure 5. Schematic of experimental configurations: unconstrained ice sample (a); toroidal ice sample constrained by external steel pipe and free to expand into central cavity (b); toroidal ice sample constrained by external and internal steel pipes (c).

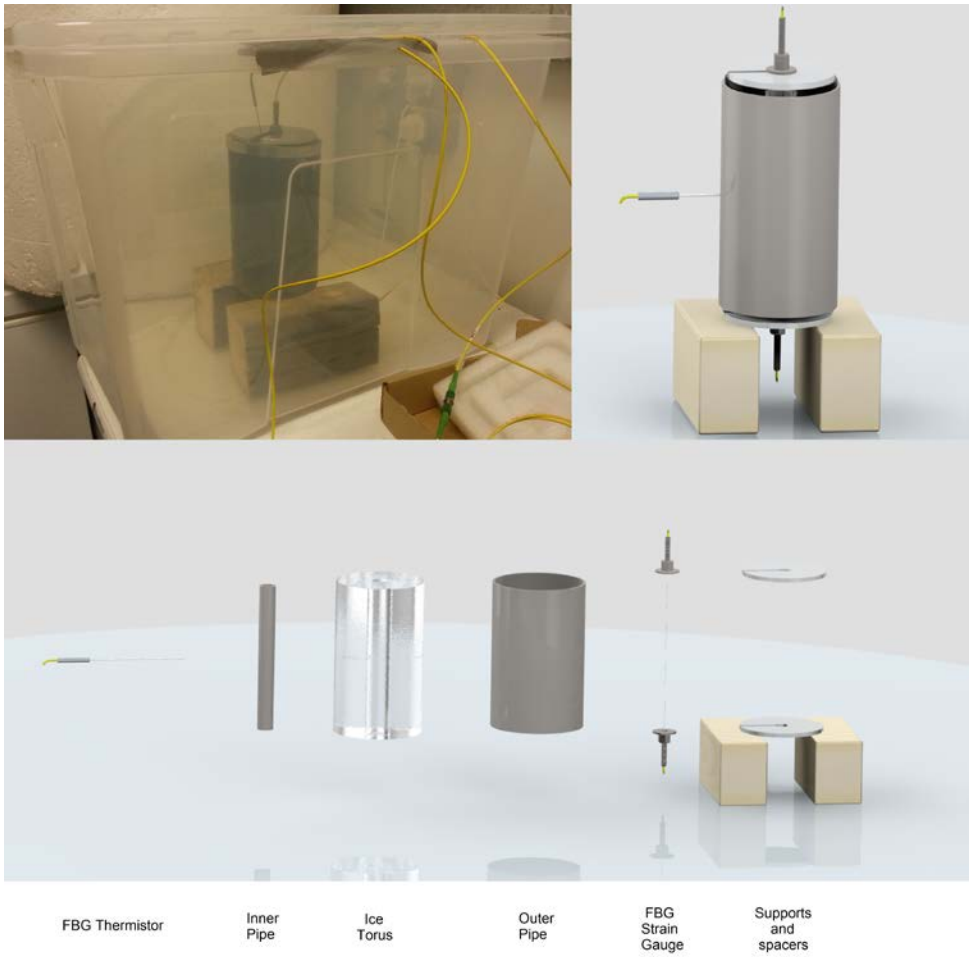

Figure 6. Full experiment photo, schematic and exploded schematic.

Thermal expansion of floating confined ice

Laboratory experiments were conducted in the UNIS cold lab ice tank to investigate the possibility of ice expansion under the influence of under-ice water pressure, without external heating or cooling. This physical mechanism is not discussed in the scientific literature. It can occur when liquid brine migrates through the ice from a relatively warm region to a relatively cold region under the influence of a pressure gradient. Lateral confinement provides a vertically directed shear force at the ice edges. This shear force is in balance with the pressure force applied to the ice bottom (Fig. 7a).

Saline ice of 8cm thickness was frozen on the surface of sea water of 1m depth with initial salinity 12ppt. The ice salinity was about 6ppt. The ice was not floating in hydrostatic equilibrium, because it cohered to the tank walls. Overpressure in the tank was created by gradually pumping air into a submerged car inner tube using an electrical pump. The pump was powered by a laboratory power supply with variable voltage so that the pumping speed could be regulated (Fig. 7a). The increase of water pressure in the tank caused ice creep in the vertical direction. However, our main interest was in measuring any extension or compression of the ice in the horizontal plane.

This extension or compression in the horizontal plane was measured with one FBG fiber optic strain sensor mounted on steel angle brackets frozen into the ice (Fig. 7b and Fig. 8a). Another FBG strain sensor was mounted on similar brackets fixed to the tank wall (Fig. 7b and Fig. 8a). This sensor recorded deformation of the tank wall under ice action. The FBG thermistor string was used to measure temperature in the air above the ice and the temperature profile in the ice. A temperature and pressure sensor SBE-39 was used to record water pressure below the ice during the experiment. The resolution of the pressure measurements was $4 \cdot 10^{-4}$ dbar. All sensors were synchronized and provided measurements with sampling interval 1s.

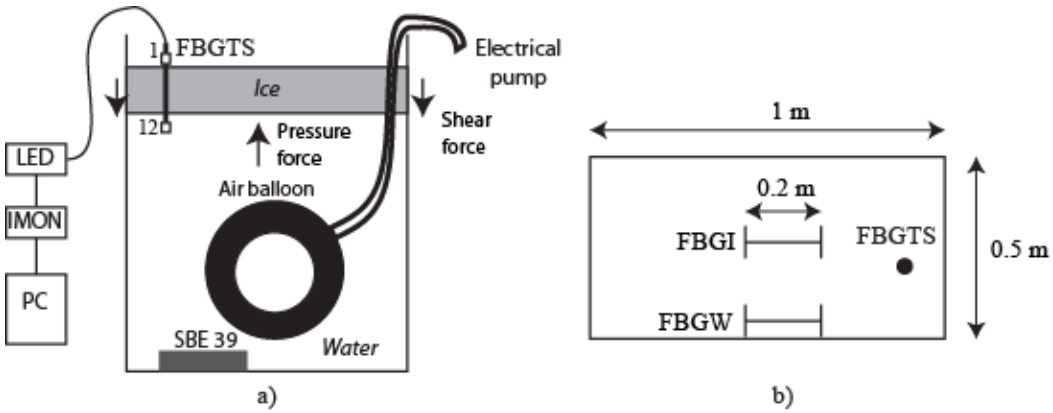

Figure 7. Scheme of the experiment on ice extension due to the water pressure increase in the ice tank (a). Locations of FBG strain sensors on the ice surface (FBGI) and on the tank wall (FBGW) (b).

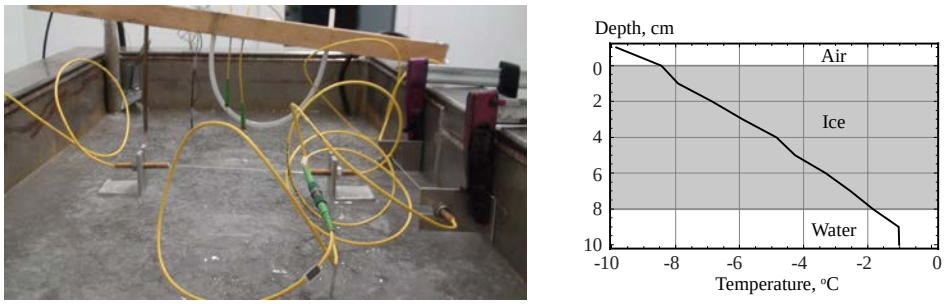

a) b)

Figure 8. Laboratory experiment in the ice tank (a). Temperature profile in model ice measured with FBG thermistor string (b).

Results of experimental studies

Thermal expansion of unconfined ice

Temperature variations in the cold laboratory cause the ice to expand and contract. The laboratory temperature is programmed into an external controller, and three programs are used.

- In the first, the control temperature is changed by 2°C every 2-3 hours or rare, over a period of several days. These are referred to as **long-term tests**.

- In the second, the control temperature is changed by 15-20°C up and down in each test twice. These tests take 4-6 hours, and are referred to as **short-term tests**.
- In the third set, the room temperature began at -20 °C, and the cooling system was then switched off. This led to an increase in temperature which was more monotonic than the other tests (where the cooling system caused sinusoidal temperature fluctuations about a long-term trend). These tests take 8 hours, and are referred to as **monotonic tests**.

The coefficient of volumetric thermal expansion of a material (CTE) is determined by the formula

$$\kappa = \frac{1}{\delta V}\frac{d\delta V}{dT}, \tag{3}$$

where δV is the infinitesimal volume of the material, and $d\delta V$ is a change of the volume caused by the temperature change from T to $T+dT$. If the sample mass $\delta m=\rho\delta V$ is conserved, definition (3) can be formulated as

$$\kappa = -\frac{1}{\rho}\frac{d\rho}{dT}. \tag{4}$$

CTE of fresh ice (CTEFI) is calculated with formula (4) where the ice density is calculated by the formula

$$\rho_i = 916.8(1+1.58\cdot 10^{-4}T)^{-1}\ (\mathrm{kg/m^3}). \tag{5}$$

CTEFI is around $1.58\cdot 10^{-5}$ K^{-1}.

In general, when saline ice includes permeable channels filled by liquid brine, the mass of a saline ice sample is not a constant, and formula (4) can't be used for the calculation of CTE for saline ice. Here, we assume that saline ice consists of ice with closed brine pockets (ICP) and permeable brine channels. ICP is not permeable by brine, and the ICP salinity is constant. Therefore CTE for ICP is calculated according to formula (4) as follows

$$\kappa_{icp} = -\frac{1}{\rho_{icp}}\frac{d\rho_{icp}}{dT}. \tag{6}$$

ICP density is calculated by the formula (Schwerdtfeger, 1963)

$$\rho_{icp} = \frac{(1-\nu)\rho_w\rho_i S}{\sigma_{icp}(\rho_i-\rho_w)+\rho_w S(1-\sigma_{icp})}, \tag{7}$$

where ρ_w= 999 kg/m^3 is the fresh water density, σ_{icp} is the ICP ice salinity, and S is the fractional salt content of the brine. For sea water brine the fractional salt content is calculated with the formulas

$$S = \alpha T\,,\ \alpha = -0.0182\ \mathrm{K}^{-1},\ T \in (0^{\circ}\mathrm{C}, -8.2^{\circ}\mathrm{C}),$$
$$S = 0.149 + (T + 8.2)\alpha',\ \alpha' = -0.01\ ^{\circ}\mathrm{C}^{-1},\ T \in (-8.2^{\circ}\mathrm{C}, -23^{\circ}\mathrm{C}). \quad (8)$$

The ICP salinity is equal to the mass of salt in the liquid brine included in closed brine pockets in a unit mass of ICP. CTE calculated with formula (6) and (7) coincides with CTE introduced by Malmgren (1927), who assumed that permeable channels are absent in sea ice.

Since saline ice includes ICP and permeable channels filled by liquid brine the total salinity is equal to a sum $\sigma_{si}=\sigma_{icp}+\sigma_{pc}$, where σ_{pc} is a mass of salt in permeable brine channels inside a unit volume of saline ice. Liquid brine located in the permeable channels doesn't influence the thermal expansion of saline ice (Cox, 1983). The salinity of the ICP is constant, but the ICP mass is changing since some closed brine pockets can transform into permeable channels due to the temperature changes. Thermal expansion of saline ice is determined by volumetric changes of the ICP which depend on both the thermal and mass changes.

Let us assume that the mass of an infinitesimal ICP sample is $\delta m_{icp}=\rho_{icp}\delta V_{icp}$ when the ICP temperature is T. The ratio of the ICP masses related to different temperatures is equal to

$$\frac{\delta m_{icp}}{\delta m_{icp,0}} = \frac{\rho_{icp}}{\rho_{icp,0}} \frac{\delta V_{icp}}{\delta V_{icp,0}}, \quad (9)$$

where the subscript "0" is related to the values of the mass, density and volume at $T=T_0$. Assuming ice isotropy and small deformations we can rewrite formula (11) in the form

$$\varepsilon_{\delta m} = \frac{\rho_{icp}}{\rho_{icp,0}}\left(1 + 3\varepsilon_{\delta L}\right) - 1, \quad (10)$$

where the relative change of the ICP mass $\varepsilon_{\delta M}$ and the linear deformation $\varepsilon_{\delta L}$ are determined by the formulas

$$\varepsilon_{\delta m} = \frac{\delta m_{icp} - \delta m_{icp,0}}{\delta m_{icp,0}},\ \varepsilon_{\delta L} = \frac{\delta L_{icp} - \delta L_{icp,0}}{\delta L_{icp,0}}. \quad (11)$$

The experiments were performed with ice samples of finite sizes. FBG sensors registered the temperature T and linear deformation ε_L of the samples depending on the time. The linear deformation of a sample is determined by the formula

$$\varepsilon_L = \frac{L(t) - L_0}{L_0}, \quad (12)$$

where L is the linear dimension of the sample, L_0 is the initial sample length, and t is the time.

The effective coefficient of linear thermal expansion (ECTE) of an ice sample is determined by the formula

$$\kappa_{si,L} = \frac{d\varepsilon_L}{dt}\left(\frac{dT}{dt}\right)^{-1}, \quad (13)$$

where the temperature $T(t)$ is registered in a point inside the sample. Temperature gradients within the sample can make it difficult to analyse equation 13. Therefore in our experiments we changed the air temperature slowly and measured the temperature with FBG thermistor-string at several points within an ice sample to control the temperature gradient over the sample.

A representative time of temperature equilibration over a sample is given by the formula

$$t_* = \frac{\rho_{si} c_{si}}{k_{si}} L_*^2, \quad (14)$$

where ρ_{si}=920 kg/m^3 is typical value of sea ice density, k_{si}= 2 W/(m·K) is a typical value of the thermal conductivity of sea ice, L_*=0.1 m is representative length of the sample, and c_{si} is the specific heat capacity of saline ice. The specific heat capacity of fresh ice is equal to 2 kJ/(kg·K). Formula 14 then gives a time of temperature equilibration in fresh ice samples of 2.5 hours.

The specific heat capacity of saline ice increases with temperature according to the formula derived by Schwerdtfeger (1963). This is because there is a greater degree of phase change, and thus a greater latent heat expenditure, at higher temperatures. For example, the specific heat capacities of saline ice with salinities 4 ppt and 8 ppt reach respectively 10.4 kJ/(kg·K) and 18.7 kJ/(kg·K) when the temperature is -3 °C. With these salinities, the times of temperature levelling should reach respectively 13 hours and 23.4 hours.

The relative change of the ICP mass ε_m in a sample is estimated with a formula similar to (10)

$$\varepsilon_m = \frac{\rho_{icp}}{\rho_{icp,0}}\left(1+3\varepsilon_L\right)-1. \quad (15)$$

Results of the long-term tests with fresh ice samples are shown in Fig. 9. The temperature change interval was 4-5 hours. Figure 9a shows temperature variations in the ice samples as measured with the FBG thermistor string. The insert graph on Fig. 9a shows temporal variations induced by the cooling cycle of the fans. The data are averaged over 15 min intervals to minimize the influence

of the fan cycle. Calculated values for ECTE for fresh ice are shown in Fig. 9b, and these are close to the CTEFI shown by the dashed line, with deviation less than 10%.

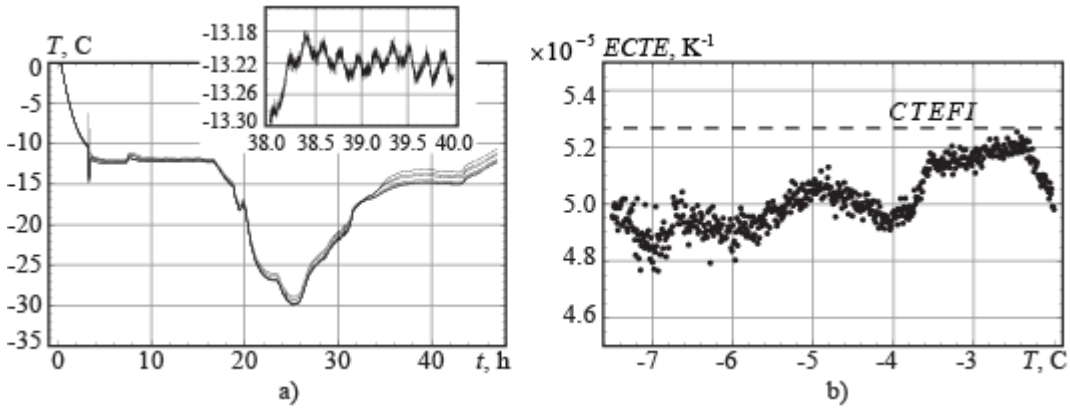

Figure 9. Temperature (a) and the coefficient of thermal expansion versus the time (b), for fresh ice sample in long-term test.

Two mixtures of sea water and fresh water were made, with respective salinities 9.4ppt and 2.3ppt. These two mixtures were frozen and prepared as ice samples: results for these samples are shown in Fig. 10-12. The experiments lasted for 190h and 415h respectively. The temperature and strain are shown as a function of time in Fig. 10. Strain is initially defined as zero. In Fig. 10a the strain and temperature gradients have opposite signs between 50 and 100h. In Fig. 10b the gradients have the same sign throughout. The opposite gradients of strain in Fig. 10a show the temperature range in which saline ice exhibits abnormal thermal expansion.

The dependency of strain on temperature is shown in Fig. 11a,b. The circles indicate the beginning of the experiments. Abnormal thermal expansion (the ice contracts with increasing temperature) is seen above around -10°C in Fig. 11a (which shows the test conducted on ice made with water of 9.4ppt salinity). The less saline sample also shows a slightly nonlinear, but still positive, ECTE (Fig. 11b). In both of the experiments hysteresis was observed in the strain-temperature curves at the points where the cycle switches from heating to cooling: similar effects were observed by Butkovich (1959) and Johnson and Metzner (1990). Figures 11c,d show the relative changes of the ICP masses ε_m in the ice samples calculated with formula (15). One can see that the ICP mass decreases with the temperature increase in the sample with salinity 9.4 ppt. The ICP mass of the sample with salinity 2.3 ppt changes in the opposite direction. Repeating thermal loading leads to the loss of the ICP mass in the both cases. This suggests that thermal cycling tends to promote open channels in the ice in favour of closed brine pockets.

Dependencies $\varepsilon_L(T)$ calculated from the experimental data were approximated by polynomial fit on different time intervals, to allow the calculation of the ECTE by formula (13). Examples of polynomial approximations are shown in Fig. 12a, and Fig. 12b shows the ECTE versus the temperature. The black squares show the ECTE calculated by Johnson and Metzner (1990) with an ice salinity of 2 ppt.

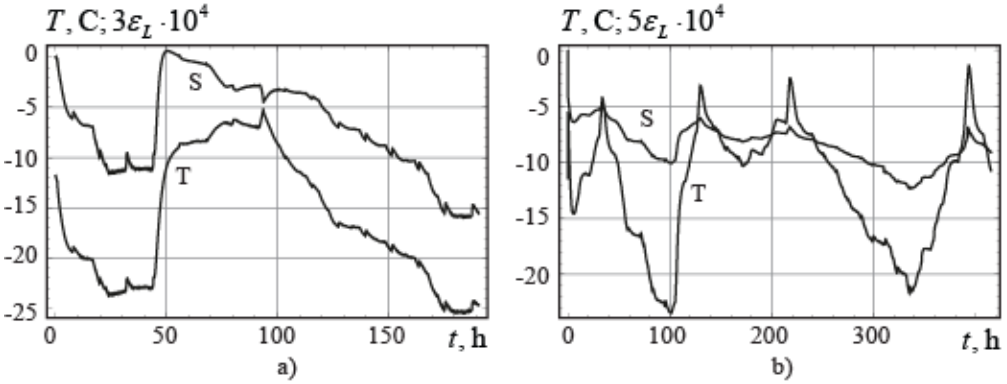

Figure 10. Temperature (T) and Strain (S) versus the time in ice samples with salinity 9.4 ppt (a) and 2.3 ppt (b). Long-term tests.

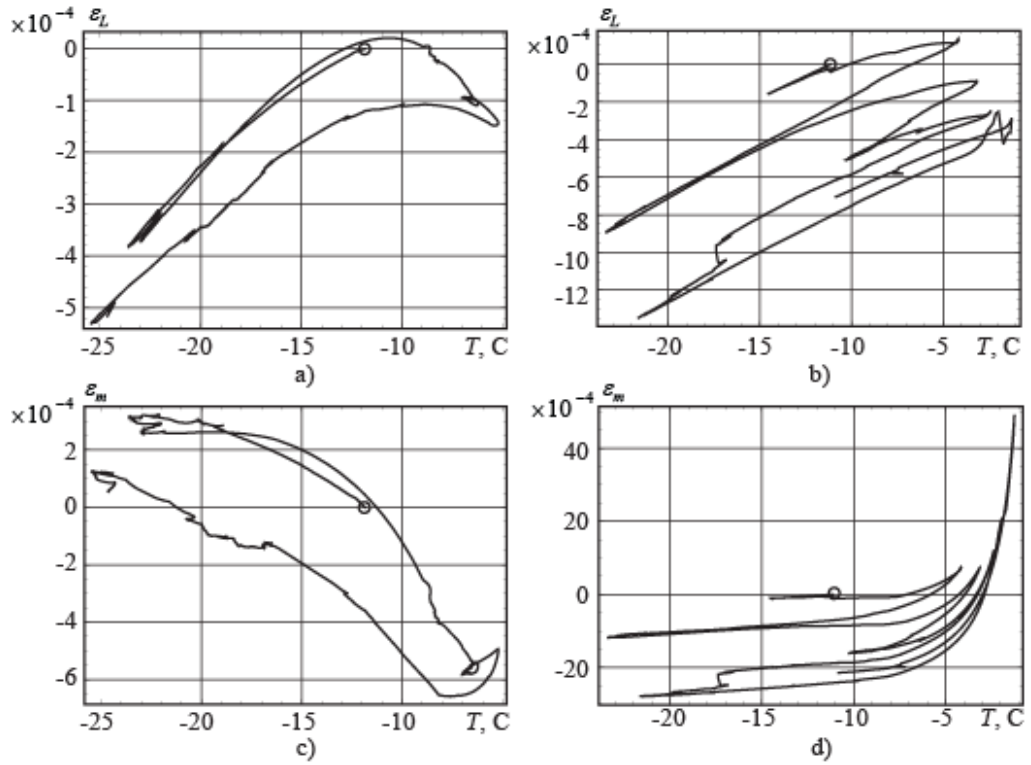

Figure 11. Strains versus temperature in ice samples with salinity 9.4 ppt (a) and 2.3 ppt (b), and the relative changes of the ICP masses of the samples with salinity 9.4 ppt (c) and 2.3 ppt (d) versus temperature. Long-term tests.

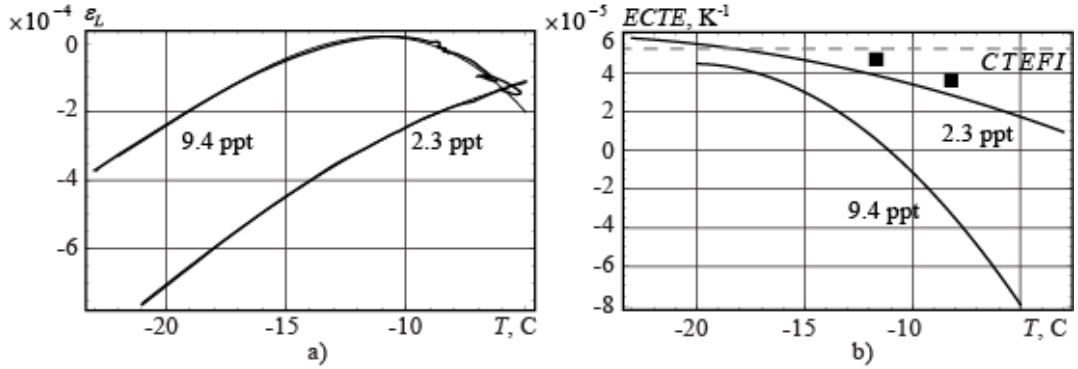

Figure 12. Polynomial approximations of the strain-temperature dependencies of ice samples (a) and ECTE versus the temperature calculated for the same samples (b). The curves are constructed with initial ice salinity 9.4 ppt and 2.3 ppt. Long-term tests.

ECTE calculated with using of the data of the long-term (the temperature change interval is 2-3 hours), short-term and monotonic tests with saline ice samples are compared in Fig. 13a. In all these tests ice samples were made from a mixture of sea and fresh water of 6 ppt salinity. Averaging of the strain-temperature curves over 15 min, and polynomial interpolation of these averages, was used to calculate ECTE on specific time intervals. Their duration was 11 hours in the long-term test, 1 hour in the short-term test and 8 hours in the monotonic test. Absolute values of the ECTE are lower than CTEFI when the temperature is lower than -4°C. The long-term test shows abnormal thermal expansion, with a negative ECTE, when the ice temperature is higher than -6°C. Short-term and monotonic tests show normal thermal expansion, with a positive ECTE. Figure 13b shows the increase of the ICP mass of the samples with the temperature increase.

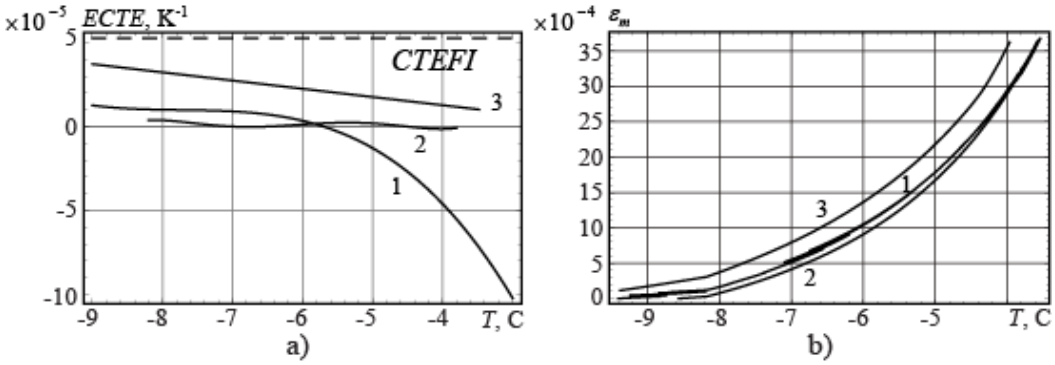

Figure 13. ECTE (a) and the ICP masses (b) versus the temperature in long-term (1), short-term (2) and monotonic (3) tests with saline ice samples. The ice salinity is 6 ppt.

Thermal expansion of confined ice

In total, 27 tests were conducted on confined ice, across the three geometries shown in Fig. 15, and for both fresh and saline ice (i.e. 6 different experimental configurations). These experiments took place in the cold rooms of University College London. Due to the complications of sharing working spaces, and running long experiments (often >24h), tests were not conducted according to a rigorous schedule but rather on an ad-hoc basis which allowed for both warming and cooling to be investigated in all configurations.

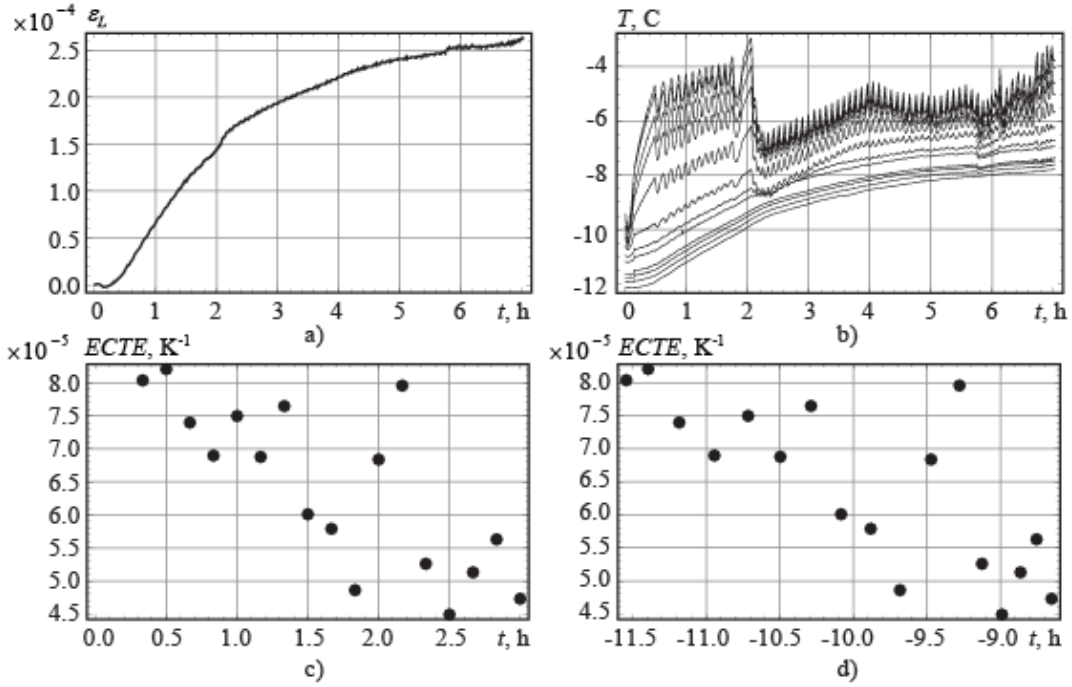

Figure 15. Results from a typical thermal expansion experiment. Strain (a) and temperature (b) measurements are shown versus the time. Calculated ECTE are shown as a function of time (c) and temperature (d). The results shown are for unconstrained fresh ice.

Figure 15 shows the results of a typical experiment. The measured strain and temperature are calculated directly from the fiber-Bragg wavelengths, using known calibration coefficients and measured wavelengths for the thermistors submersed in 0°C iced water. These measurements are shown in Fig. 15a,b. In the temperature plot we can see two minor sources of error; variations in the air temperature due to the cold room fan cycle (duration 5 minutes), and a sudden cooling (just after 12.00) when the door to an adjoining cold room was opened. Neither of these processes has a strong effect on the observed in-ice temperatures (the lowest six lines on the top right plot) but both will have some effect on overall results.

Calculated ECTEs are shown in Fig. 15c,d. For these, ice temperature and strain are averaged over 600s periods. If the temperature difference in this window is less than 0.1°C then the measurement is ignored, since slight residual strains at constant temperatures can lead to high anomalous expansion coefficients. The results shown are therefore those for which the temperature difference across the measurement window was sufficiently high. These are then shown as a function of time and temperature.

Figure 16 shows results combined across all experiments. For fresh ice (Fig. 16a) there is a range of positive values of ECTE, with a few negative outliers. We see no clear trend with temperature. Average ECTE are $46.9 \times 10^{-6} K^{-1}$ for unconstrained fresh ice, $26.9 \times 10^{-6} K^{-1}$ for ice constrained by an external pipe, and $64.3 \times 10^{-6} K^{-1}$ for ice constrained by both internal and external pipes. The average for the unconstrained pipe is within 10% of the literature value. For saline ice with no pipe (average value $52.4 \times 10^{-6} K^{-1}$) and with 1 pipe (average $50.6 \times 10^{-6} K^{-1}$)

we see similar behavior. For saline ice (Fig. 16b) with two pipes the values over the first eight hours of the test are similar (average 54.2 x$10^{-6}K^{-1}$, but then we see a clear trend towards negative ECTE with rising temperature (above around -10°C). It may be that the dual pipes prevent brine drainage, and the phase changes associated with trapped brine drive the negative thermal expansion coefficient. The conditions at the surface of the ice can affect thermal expansion by constraining the ice as well as by constraining the brine. We believe that the high scatter seen in our results may be due to residual stresses which build up and relax in the ice over time, particularly as it sticks against the pipes. These residual stresses may be released later than they build up, which would mean that the correlation between observed ice strain and instantaneous temperature is less clear than if all strains are realized immediately.

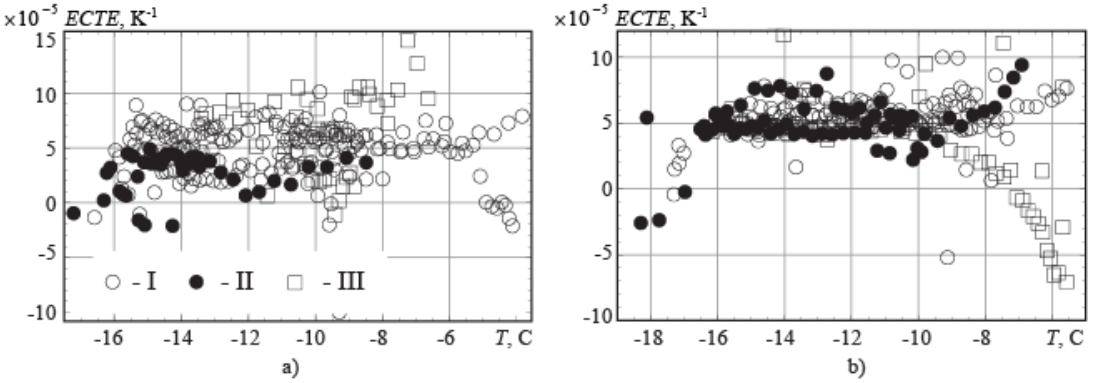

Figure 16. Experimentally measured ECTE, plotted as a function of temperature for fresh ice (a), and for saline ice (b). I - unconstrained sample; II –sample with one pipe; and III – sample with two pipes.

Thermal expansion of floating confined ice

The effects of under-ice pressure on a confined ice sheet are shown in Fig. 17. As the pressure was gradually increased in the water the strain in the ice also increased (Fig. 17a). At the same time the strain measured on the inside face of the wall decreased, indicating that the wall bent outwards slightly. The temperature at 1cm depth and deeper increased as a result of water migrating through the ice sheet (Fig. 17b). This water migration was also visually observed. The decrease in the surface temperature is related to the overall temperature changes in the cold lab. This effect is also picked up by the thermistor at a depth of 1cm, after around 500s.

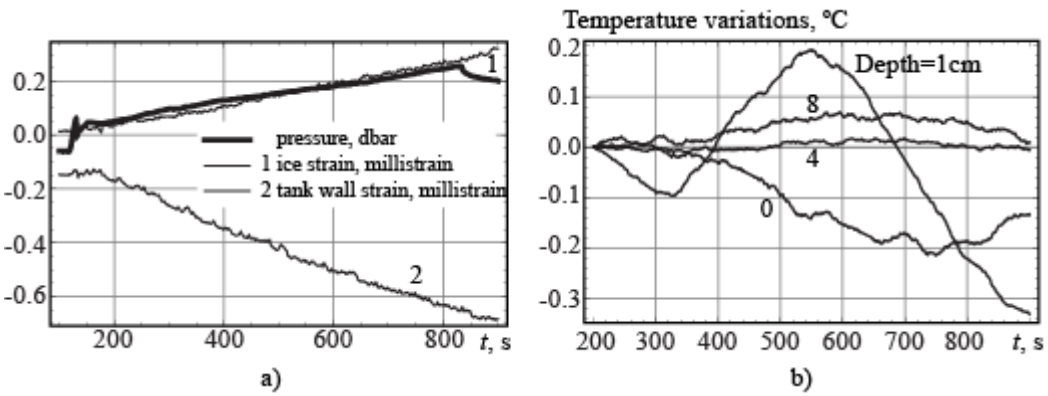

Figure 17. Strains in ice and tank walls induced by the increase of the water pressure below the ice (a). Temporal variations of the ice temperature induced by brine migration through the ice (b).

Figure 17a shows positive thermal expansion of ice caused by the vertical migration of liquid brine through the ice (which has a vertical temperature gradient.) Under-ice pressure drives the brine upwards. The brine temperature is initially equal to the temperature of its surrounding ice, since the brine is in local thermodynamic equilibrium with ice. Therefore, as brine migrates upward, warmer brine from the bottom of the ice (where the ice is warmest) heats up the top layers of the ice. From Fig. 17, ice deformation reaches about $2 \cdot 10^{-4}$ when the temperature increases by about 0.1°C. This deformation is caused by thermal expansion of ice and ice compression between the tank walls. The conclusion here is that if brine is forced vertically upwards through the ice, this is likely to warm the ice (since the sea water and lower brine are warm compared to the brine near the upper surface), leading to an expansion.

Conclusions

FBG sensors are a productive tool for laboratory measurements of the thermo-mechanical properties of saline ice. It was possible to perform experiments with samples of different sizes and geometries. The high sampling frequency, accuracy and resolution of the FBG sensors provided good quality data across a temperature range from 0°C to -20°C. The sensors, and their associated hardware and software, were stable and robust. The main complication in these experiments was in developing techniques to mount the FBG sensors onto the ice samples.

In this paper we have compared values of the coefficients of linear thermal expansion calculated from laboratory experiments (ECTE) to predictions based on a model of ice as an impermeable medium (to liquid brine) and on a fresh ice model. Negative values of ECTE were found when the ice samples had salinities of 6ppt, 8ppt and 9.4ppt. Abnormal thermal expansion – contraction with increasing temperature - was observed at temperatures higher than -8°C (6ppt and 8ppt experiments) or -11°C (9.4ppt experiments). Hysteresis effects, similar to those described in earlier work, were observed. Surface area to volume ratio, and confinement of the ice, appear to affect the ECTE. In experiments with confined floating ice we observed heating and thermal expansion of ice due to the vertical migration of liquid brine through the ice under the action of water pressure beneath the ice.

We formulated a new model of saline ice consisting of the ice with closed brine pockets (ICP) and permeable brine channels, and assumed that closed brine pockets can transform into permeable channels under temperature changes. This process may influence the fraction of the mass contained in closed pockets (the ICP mass). Using experimental data we estimated changes of the ICP mass of the ice samples with different salinity. It was discovered that the ICP mass decreases with increasing temperature in ice samples of high salinity (9.4 ppt), and the ICP mass increases with increasing temperature in ice samples with

salinity 6 ppt and 2,3 ppt. Repeated or cycling temperature changes influence the decrease in ICP mass with time in all samples.

The authors wish to acknowledge the support of the Research Council of Norway through SFI SAMCoT.

References

Butkovich, T.R., 1959. Thermal expansion of ice. Journal of Applied Physics, 30(3), 350-353.

Cox G.F.N., 1983. Thermal expansion of saline ice. Journal of Glaciology, 29(103), 425-432.

Ferraro, P., De Natale, G., 2002. On the possible use of optical fiber Bragg gratings as strain sensors for geodynamical monitoring. Optics and Lasers in Engineering**, 37** (2-3), 115–130.

Golden, K.M., Eicken, H., Heaton, A.L., Miner, J., Pringle, D.J., Zhu, J., 2007. Thermal evolution of permeability and microstructure in sea ice. Geophysical Research Letters, Vol. 34, L 16501.

Johnson J.B., Metzner R.C., 1990. Thermal expansion coefficients for sea ice. Journal of Glaciology, 36(124), 343-349.

Lishman, B., Marchenko, A., 2014. An investigation of relative thermal expansion and contraction of ice and steel. Proc. of the 22th IAHR Symposium on Ice, Singapore, paper 1173.

Malmgren, F., 1927. On the properties of sea ice. The Norwegian North Polar Expedition with
the ”Maud”, 1918-1925, 1(5).

Marchenko, A., Thiel, T., Sukhorukov, S., 2012. Measurements of Thermally Induced Deformations in Saline Ice with Fiber Bragg Grating Sensors. 21st IAHR International Symposium on Ice "Ice Research for a Sustainable Environment", Li and Lu (ed.), Dalian University of Technology Press, Dalian, ISBN 978-7-89437-020-4, 651-659.

Marchenko, A., Wrangborg, D., Thiel., T., 2013. Using distributed optical fiber sensors based on FBGs for the measurement of temperature fluctuations in saline ice and water on small scales. POAC13-134, Espoo, Finland, 11 pp.

Mueller, B., Meissner, J., Thiel, T., 2006. Results of continuous in-situ stress measurement with optical strain sensors. In-situ Rock stress, London: Taylor & Francis Group, 249-256.

Othonos, A., Kalli, K., 1999. Fiber Bragg Gratings: Fundamentals and Applications in Telecommunications and Sensing. Artech House, ISBN 0-89006-344-3.

Petterson, O., 1883. On the properties of water and ice. In Nordenskiold, ed. Vega-expeditionens veisnskapliga iakttagelser. Bd. 2. Stockholm, F. and G. Beijers Forlag, 247-323.

Rao, Y.J., 1997. In-fiber Bragg grating sensors. Measurement Science and Technology, 8(4), Sci. Technol., 8, 355-376.

Schwerdtfeger, P., 1963. The thermal properties of sea ice. J. Glaciol. 4 (36), 789–807.

Weeks, W. F., Ackley, S.F., 1986. The growth, structure and properties of sea ice, in The Geophysics of Sea Ice, edited by N. Untersteiner, pp. 9 –164, Plenum, New York.

Wrangborg, D., Marchenko, A., 2015. Measurement of Loads Exerted by Sea Ice on the Quay at Kapp Amsterdam on Svalbard. POAC15-141, Trondheim, Norway, 9 pp.

"The authors declare that there is no conflict of interest regarding the publication of this paper".